nature geoscience

LETTERS

PUBLISHED ONLINE: 24 AUGUST 2015 | DOI: 10.1038/NGEO2502

Orbitally forced ice sheet fluctuations during the Marinoan Snowball Earth glaciation

Douglas I. Benn[1,2]*, Guillaume Le Hir[3], Huiming Bao[4], Yannick Donnadieu[5], Christophe Dumas[5], Edward J. Fleming[1,6†], Michael J. Hambrey[7], Emily A. McMillan[6], Michael S. Petronis[8], Gilles Ramstein[5], Carl T. E. Stevenson[6], Peter M. Wynn[9] and Ian J. Fairchild[6]

Two global glaciations occurred during the Neoproterozoic. Snowball Earth theory posits that these were terminated after millions of years of frigidity when initial warming from rising atmospheric CO_2 concentrations was amplified by the reduction of ice cover and hence a reduction in planetary albedo[1,2]. This scenario implies that most of the geological record of ice cover was deposited in a brief period of melt-back[3]. However, deposits in low palaeo-latitudes show evidence of glacial–interglacial cycles[4–6]. Here we analyse the sedimentology and oxygen and sulphur isotopic signatures of Marinoan Snowball glaciation deposits from Svalbard, in the Norwegian High Arctic. The deposits preserve a record of oscillations in glacier extent and hydrologic conditions under uniformly high atmospheric CO_2 concentrations. We use simulations from a coupled three-dimensional ice sheet and atmospheric general circulation model to show that such oscillations can be explained by orbital forcing in the late stages of a Snowball glaciation. The simulations suggest that while atmospheric CO_2 concentrations were rising, but not yet at the threshold required for complete melt-back, the ice sheets would have been sensitive to orbital forcing. We conclude that a similar dynamic can potentially explain the complex successions observed at other localities.

The Wilsonbreen Formation in northeast Svalbard contains a detailed record of environmental change during the Marinoan, the second of the major Cryogenian glaciations (650–635 Ma; refs 7,8). At this time, Svalbard was located in the Tropics on the eastern side of Rodinia[9,10]. The <180 m thick Wilsonbreen Formation was deposited within a long-lived intracratonic sedimentary basin[11]. It is subdivided into three members (W1, W2 and W3) based on the relative abundance of diamictite and carbonate beds[7,8] (Fig. 1 and Supplementary Figs 1 and 2). The occurrence throughout the succession of lacustrine sediments containing both precipitated carbonate and ice-rafted detritus, and intermittent evaporative carbonates and fluvial deposits, indicates that the basin remained isolated from the sea, consistent with eustatic sea-level fall of several hundred metres and limited local isostatic depression (Supplementary Information; ref. 12). This makes it ideal for investigating environmental change within a Neoproterozoic panglaciation, as it provides direct evidence of subaerial environments and climatic conditions.

We made detailed sedimentary logs at ten known and new localities extending over 60 km of strike (Fig. 1 and Supplementary Fig. 1; see Methods). Seven sediment facies associations were identified, recording distinct depositional environments that varied in spatial extent through time (Supplementary Fig. 3 and Supplementary Information). These are: FA1: subglacial, recording direct presence of glacier ice; FA2: fluvial channels; FA3: dolomitic floodplain, recording episodic flooding, evaporation and microbial communities; FA4: carbonate lake margin, including evidence of wave action; FA5: carbonate lacustrine, including annual rhythmites and intermittent ice-rafted debris; FA6: glacilacustrine, consisting of ice-proximal grounding-line fans (FA6-G) and ice-distal rainout deposits (FA6-D); and FA7: periglacial, recording cold, non-glacial conditions. Further descriptions are provided in the Supplementary Information. The vertical and horizontal distribution of these facies associations (Fig. 1) allows the sequence of environmental changes to be reconstructed in detail:

(1) The base of the Wilsonbreen Formation is a well-marked periglacially weathered horizon with thin wind-blown sands (Supplementary Fig. 4a,b). This surface records very limited sediment cycling in cold, arid conditions.
(2) At all localities, the weathering horizon is overlain by fluvial channel facies (FA2) and mudstones, marking the appearance of flowing water in the basin and implying positive air temperatures for at least part of the time (Supplementary Fig. 5a).
(3) Glacilacustrine deposits (FA6-D) record flooding of the basin and delivery of sediment by ice rafting (Supplementary Fig. 4c,d). Far-travelled clasts are common, indicating transport by a large, continental ice sheet.
(4) Warm-based, active ice advanced into the basin, indicated by traction tills and glacitectonic shearing (FA1; Supplementary Fig. 4e–g). (1–4 make up Member W1).
(5) Ice retreat is recorded by a second periglacial weathering surface (FA7). This is overlain by fluvial channel, floodplain, lake-margin and carbonate lacustrine sediments of W2 (FA2-5; Supplementary Fig. 5), recording a shifting mosaic of playa lakes and ephemeral streams. Lakes and river channels supported microbial communities. Millimetre-scale carbonate-siliciclastic rhythmites indicate seasonal cycles of

[1]Department of Geology, The University Centre in Svalbard (UNIS), N-9171 Longyearbyen, Norway. [2]School of Geography and Geosciences, University of St Andrews, St Andrews KY16 8YA, UK. [3]Institut de Physique du Globe de Paris, 75238 Paris, France. [4]Department of Geology and Geophysics, E235 Howe-Russell Complex, Louisiana State University, Baton Rouge, Louisiana 70803, USA. [5]Laboratoire des Sciences du Climat et de l'Environnement, CNRS-CEA, 91190 Gif-sur-Yvette, France. [6]School of Geography, Earth and Environmental Sciences, University of Birmingham, Birmingham B15 2TT, UK. [7]Institute of Geography and Earth Sciences, Aberystwyth University, Aberystwyth SY23 3DB, UK. [8]Natural Resource Management, Environmental Geology, New Mexico Highlands University, Las Vegas, New Mexico 87701, USA. [9]Lancaster Environment Centre, University of Lancaster, Lancaster LA1 4YQ, UK. †Present address: CASP, West Building, 181A Huntingdon Road, Cambridge CB3 0DH, UK. *e-mail: Doug.Benn@unis.no

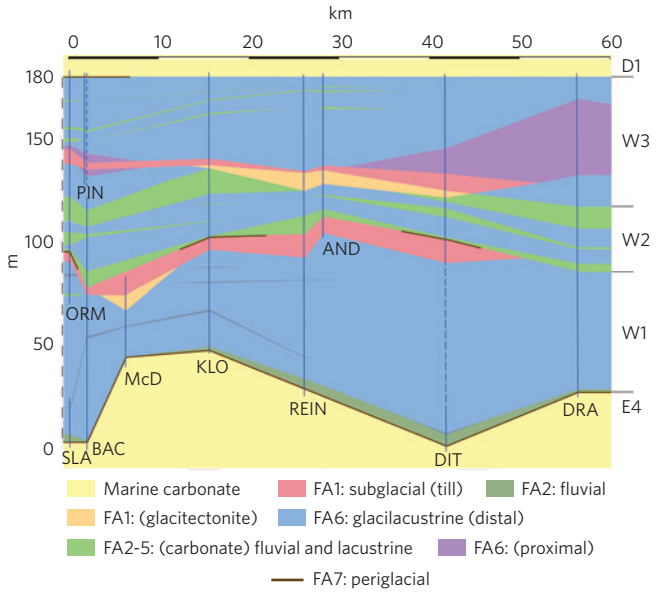

Figure 1 | Sedimentary architecture and palaeoenvironments of the Wilsonbreen Formation. Regional correlation of facies associations and members W1, W2 and W3 across northeast Svalbard. From north to south, study locations are: DRA, Dracoisen; DIT, Ditlovtoppen; AND, East Andromedafjellet; REIN, Reinsryggen (informal name); KLO, Klofjellet; McD, MacDonaldryggen; BAC, Backlundtoppen–Kvitfjellet ridge; PIN, Pinnsvinryggen (informal name); SLA, Slangen and ORM, Ormen.

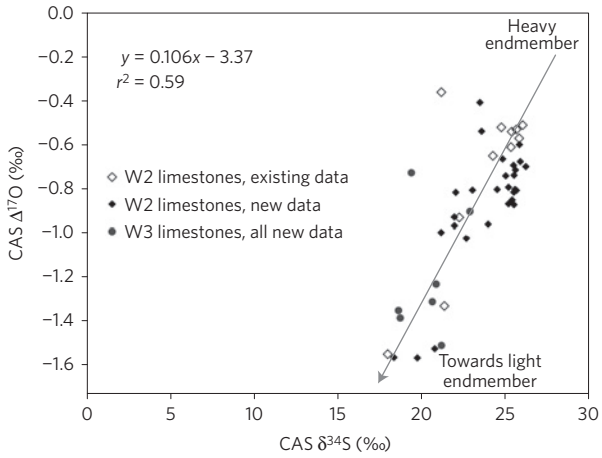

Figure 2 | Co-variation of $\Delta^{17}O$ and $\delta^{34}S$ from carbonate-associated sulphate in W2 and W3. 'Existing data' (ref. 16) and new data define a mixing line between pre-glacial sulphate (top) and an isotopically light sulphate formed by oxidation of pyrite including incorporation of a light-$\Delta^{17}O$ signature from a CO_2-enriched atmosphere. Data from W2 and W3 lie on closely similar trend lines, indicating no detectable change in p_{CO_2} between deposition of the two members.

photosynthesis. The environment seems to have been closely similar to that of the present-day McMurdo Dry Valleys in Antarctica, although with less extreme seasonality owing to its low latitude[13].

(6) Water levels and glacier extent underwent a series of oscillations, recorded by switches between glacilacustrine diamictite (FA6-D) and fluvial, lacustrine and lake-margin sediments (FA2-5) in W2. Sedimentation rates inferred from annual rhythmites in W2 suggest that each retreat phase may have lasted $\sim 10^4$ years.

(7) A second major ice advance marks the base of W3, with widespread deposition of subglacial tills and glacitectonism of underlying sediments. Basal tills are absent from the northernmost locality, but close proximity of glacier ice is recorded by grounding-line fans (FA6-G; Supplementary Fig. 4h,i).

(8) Ice retreated while the basin remained flooded and glacigenic sediment continued to be delivered to the lake by ice rafting. Thin laminated carbonates (FA5) in W3 indicate periods of reduced glacigenic sedimentation, indicative of minor climatic fluctuations over timescales of $\sim 10^3$ years (Supplementary Fig. 5g).

(9) A sharp contact with overlying laminated 'cap' carbonate (Supplementary Fig. 2) records the transition to post-glacial conditions. At some localities, basal conglomerates provide evidence of subaerial exposure, followed by marine transgression. The cap carbonate closely resembles basal Ediacaran carbonates elsewhere, and marks global deglaciation, eustatic sea-level rise and connection of the basin to the sea[1,12,14].

Environmental and atmospheric conditions during deposition of W2 and W3 can be further elucidated by isotopic data from carbonate-associated sulphate in lacustrine limestones (Fig. 2 and Supplementary Fig. 6). These exhibit negative to extremely negative $\Delta^{17}O$ values, with consistent linear co-variation with $\delta^{34}S$, indicating mixing of pre-glacial sulphate and isotopically light sulphate formed in a CO_2-enriched atmosphere[15,16]. The observed values could reflect non-unique combinations of p_{CO_2}, p_{O_2}, O_2 residence time and other factors, but a box model[17] indicates p_{CO_2} was most likely ~10 to 100 mbar (1 mbar = 1,000 ppmv).

These values are far too high to permit formation of low-latitude ice sheets in the Neoproterozoic, but they are consistent with a late-stage Snowball Earth. For an ice-free Neoproterozoic Earth, model studies indicate mean terrestrial temperatures in the range 30–50 °C for $p_{CO_2} = 10$ to 100 mbar (ref. 18). Formation of low-latitude ice sheets requires much lower p_{CO_2}, on the order of 0.1–1 mbar (refs 2,19,20). Once formed, however, ice sheets can persist despite rising CO_2 from volcanic outgassing, as a result of a high planetary albedo. This hysteresis in the relationship between p_{CO_2} and planetary temperature is a key element of Snowball Earth theory. It implies that W2 and W3 were deposited relatively late in the Marinoan, after volcanic outgassing had raised p_{CO_2} from 0.1 or 1 mbar to 10 or 100 mbar. Modelled silicate weathering and volcanic outgassing rates indicate that this would require 10^6 to 10^7 years[21].

The consistent co-variation of $\Delta^{17}O$ and $\delta^{34}S$ in lacustrine limestones in both W2 and W3 suggests no detectable rise in atmospheric p_{CO_2}, as this would alter the slope of the mixing line (Fig. 2). This implies that the glacier oscillations recorded in W2 and W3 occurred during a relatively short time interval ($<10^5$ years[21]) towards the end of the Marinoan. In turn, this implies that the remainder of the Wilsonbreen Formation (including the basal weathering horizon) represents many millions of years, during which p_{CO_2} built up from the low values necessary for inception of low-latitude glaciation to those indicated by the geochemical evidence. The weathering horizon provides direct evidence of cold, arid conditions during this interval, before the appearance of fluvial and glacilacustrine sediments in the basin.

The evidence for ice sheet advance/retreat cycles at low latitudes in a CO_2-enriched atmosphere motivated a series of numerical simulations to test the hypothesis that these cycles were linked to Milankovitch orbital variations. We employed asynchronous coupling of a three-dimensional ice sheet model and an atmospheric general circulation model using the continental configuration of ref. 22. We first ran simulations with a modern orbital configuration to examine ice sheet behaviour through a large range of p_{CO_2} values from 0.1 to 100 mbar (ref. 23; Supplementary Figs 7–10). Consistently with previous results[2,20], at low p_{CO_2} (0.1 mbar), global ice volume reaches 170×10^6 km^3, but substantial tropical land

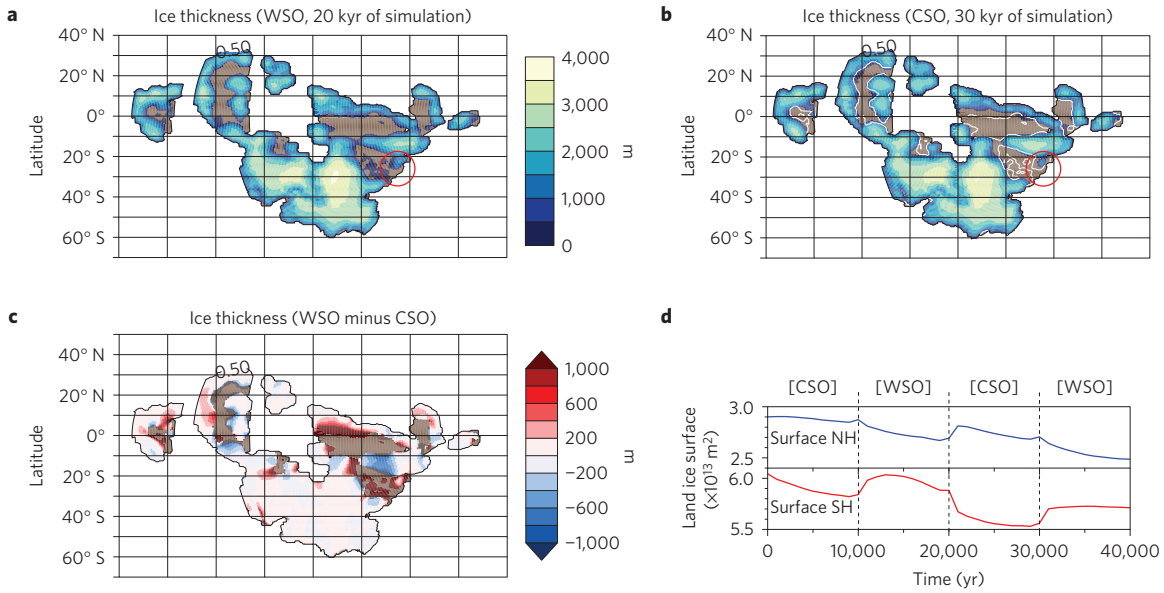

Figure 3 | Modelled ice sheet oscillations in response to orbital forcing. a,**b**, Shaded contours show land ice thickness obtained with 20 mbar of carbon dioxide in response to changes of orbital forcing (WSO (**a**)) and CSO (**b**), warm/cold summer orbit for the northern hemisphere) over the course of two precession cycles (40 kyr of simulation). In the light brown continental areas without ice, the white line is used to represent the old ice sheet extension (WSO case). The Svalbard area is indicated by a red circle. **c**, Ice thickness variation in 10 kyr (WSO case after 20 kyr minus CSO case after 30 kyr of simulation). In **a**–**c** the continental outline is shown by the 0.5 m elevation contour. **d**, Surface of hemisphere covered by ice (m^2) through time ([WSO] and [CSO] indicate which orbital configuration is used).

areas remain ice free as a result of sublimation exceeding snowfall (Supplementary Fig. 10a). Ice volume remains relatively constant for $p_{CO_2} = 0.1$ to 20 mbar (Supplementary Fig. 10b), owing to an increase in accumulation that compensates for higher ablation rates (Supplementary Fig. 13). In contrast, above 20 mbar, ice extent in the eastern Tropics significantly decreases (Supplementary Fig. 10c). At $p_{CO_2} = 100$ mbar, most of the continental ice cover disappears, except for remnants over mountain ranges (Supplementary Fig. 10d).

To test the sensitivity of the tropical ice sheets to Milankovitch forcing, experiments with changing orbital parameters were initialized using the steady-state ice sheets for $p_{CO_2} = 20$ mbar. Although obliquity has been invoked as a possible cause of Neoproterozoic glaciations[24], this mechanism remains problematical and cannot account for significant climatic oscillations at low latitudes[25,26]. We therefore focused on precession as a possible driver, and used two opposite orbital configurations, favouring cold and warm summers, respectively, over the northern tropics (CSO: cold summer orbit and WSO: warm summer orbit; Supplementary Fig. 14). Switching between these configurations causes tropical ice sheets to advance/retreat over several hundred kilometres in 10 kyr (Supplementary Movie 1), with strong asymmetry between hemispheres (Fig. 3). Shifting from WSO to CSO causes ice retreat in the Southern Hemisphere and ice sheet expansion in the Northern Hemisphere (Supplementary Fig. 14c,d). Significant ice volume changes occur between 30° N and S, but are less apparent at higher latitudes. This reflects higher ablation rates in the warmer low latitudes (Supplementary Fig. 14e,h), and higher ice sheet sensitivity to shifting patterns of melt. Larger greenhouse forcing at the end of the Snowball event implies increasing ice sheet sensitivity to subtle insolation changes. Given a strong diurnal cycle[23], our simulations also predict a significant number of days above 0 °C in the tropics (Supplementary Fig. 15), consistent with geological evidence for ice rafting, liquid water in lakes and rivers, and photosynthetic microbial communities.

Our results show that geological evidence for glacial–interglacial cycles[5–7] is consistent with an enriched Snowball Earth theory. Termination of the Marinoan panglaciation was not a simple switch from icehouse to greenhouse states, but was characterized by a climate transition during which glacial cycles could be forced by Milankovitch orbital variations. The geochemical evidence presented here implies that at least the upper 60–70% of the Wilsonbreen Formation was deposited in ~10^5 years, on the assumption that a trend in p_{CO_2} would be evident over longer timescales[21]. Rates of CO_2 build-up, however, may have slowed in the later stages of Snowball Earth owing to silicate weathering of exposed land surfaces, so it is possible that the oscillatory phase was more prolonged.

Initiation of low-latitude glaciation in the Neoproterozoic requires low p_{CO_2} (0.1–1 mbar; refs 2,19,20), implying that the oscillatory phase was preceded by a prolonged colder period (~10^6 to 10^7 years) during which p_{CO_2} increased gradually as a result of volcanic outgassing[21]. This timescale is in agreement with recent dates indicating the Marinoan lasted ~15 million years[27]. The basal weathering horizon is consistent with a period of low temperatures and limited hydrologic cycle before the oscillatory phase[2,19].

Further work is needed to refine the upper and lower limits of p_{CO_2} conducive to climate and ice sheet oscillations in Snowball Earth. Factors not included in the present model, such as supraglacial dust or areas of ice-free tropical ocean[28–30], can be expected to make the Earth system more sensitive to orbital forcing. While many details remain to be investigated, our overall conclusions remain robust.

The Neoproterozoic Snowball Earth was nuanced, varied and rich. We anticipate that detailed studies of the rock record in other parts of the world, in conjunction with numerical modelling studies, will continue to yield insight into the temporal and regional diversity of this pivotal period in Earth history.

Methods

Methods and any associated references are available in the online version of the paper.

Received 17 February 2015; accepted 8 July 2015;
published online 24 August 2015

References

1. Hoffman, P. F. & Schrag, D. P. The Snowball Earth hypothesis: Testing the limits of global change. *Terra Nova* **14,** 129–155 (2002).
2. Donnadieu, Y., Goddéris, Y. & Le Hir, G. *Treatise on Geochemistry* 2nd edn, Vol. 6, 217–229 (Elsevier, 2014).
3. Hoffman, P. F. Strange bedfellows: Glacial diamictite and cap carbonate from the Marinoan (635 Ma) glaciation in Namibia. *Sedimentology* **58,** 57–119 (2011).
4. Allen, P. A. & Etienne, J. L. Sedimentary challenge to Snowball Earth. *Nature Geosci.* **1,** 817–825 (2008).
5. Rieu, R., Allen, P. A., Plötze, M. & Pettke, T. Climatic cycles during a Neoproterozoic "snowball" glacial epoch. *Geology* **35,** 299–302 (2007).
6. Le Heron, D. P., Busfield, M. E. & Kamona, F. An interglacial on snowball Earth? Dynamic ice behaviour revealed in the Chuos Formation, Namibia. *Sedimentology* **60,** 411–427 (2013).
7. Fairchild, I. J. & Hambrey, M. J. Vendian basin evolution in East Greenland and NE Svalbard. *Precambrian Res.* **73,** 217–233 (1995).
8. Halverson, G. P. in *Neoproterozoic Geobiology and Paleobiology* (eds Xiao, S. & Kaufman, A. J.) 231–271 (Springer, 2006).
9. Li, X.-X., Evans, D. A. & Halverson, G. P. Neoproterozoic glaciations in a revised global palaeogeography from the breakup of Rodinia to the assembly of Gondwanaland. *Sedim. Geol.* **294,** 219–232 (2013).
10. Petronis, M. S. *et al.* in *AGU Fall Meeting 2013* Abstract #GP41A-1107 (American Geophysical Union, 2013).
11. Harland, W. B. *The Geology of Svalbard* (Geological Society, 1997).
12. Creveling, J. R. & Mitrovica, J. X. The sea-level fingerprint of a Snowball Earth deglaciation. *Earth Planet. Sci. Lett.* **399,** 74–85 (2014).
13. Lyons, W. B. *et al.* The McMurdo Dry Valleys long-term ecological research program: New understanding of the biogeochemistry of the Dry Valley lakes: A review. *Polar Geogr.* **25,** 202–217 (2001).
14. Hoffman, P. *et al.* Are basal Ediacaran (635 Ma) basal 'cap dolostones' diachronous? *Earth Planet. Sci. Lett.* **258,** 114–131 (2007).
15. Fairchild, I. J., Hambrey, M. J., Spiro, B. & Jefferson, T. H. Late Proterozoic glacial carbonates in northeast Spitsbergen: New insights into the carbonate-tillite association. *Geol. Mag.* **126,** 469–490 (1989).
16. Bao, H., Fairchild, I. J., Wynn, P. M. & Spötl, C. Stretching the envelope of past surface environments: Neoproterozoic glacial lakes from Svalbard. *Science* **323,** 119–122 (2009).
17. Cao, X. & Bao, H. Dynamic model constraints on oxygen-17 depletion in atmospheric O_2 after a snowball Earth. *Proc. Natl Acad. Sci. USA* **110,** 14546–14550 (2013).
18. Le Hir, G. *et al.* The snowball Earth aftermath: Exploring the limits of continental weathering processes. *Earth Planet. Sci. Lett.* **277,** 453–463 (2009).
19. Pierrehumbert, R., Abbot, D. S., Voigt, A. & Koll, D. Climate of the Neoproterozoic. *Ann. Rev. Earth Planet. Sci.* **39,** 417–460 (2011).
20. Pollard, D. & Kasting, J. F. in *The Extreme Proterozoic: Geology, Geochemistry, and Climate* (eds Jenkins, G. S., McMenamin, M. A. S., McKay, C. P. & Sohl, L.) 91–105 (Geophysical Monograph Series 146, American Geophysical Union, 2004).
21. Le Hir, G., Ramstein, G., Donnadiieu, Y. & Goddéris, Y. Scenario for the evolution of atmospheric p_{CO_2} during a snowball Earth. *Geology* **36,** 47–50 (2008).
22. Hoffman, P. F. & Li, Z. X. A palaeogeographic context for Neoproterozoic glaciation. *Palaeogeogr. Palaeoclimatol. Palaeoecol.* **277,** 158–172 (2009).
23. Pierrehumbert, R. T. Climate dynamics of a hard Snowball Earth. *J. Geophys. Res.* **110,** D01111 (2005).
24. Spiegl, T. C., Paeth, H. & Frimmel, H. E. Evaluating key parameters for the initiation of a Neoproterozoic Snowball Earth with a single Earth System Model of intermediate complexity. *Earth Planet. Sci. Lett.* **415,** 100–110 (2015).
25. Donnadieu, Y., Ramstein, G., Fluteau, F., Besse, J. & Meert, J. Is high obliquity a plausible cause for Neoproterozoic glaciations? *Geophys. Res. Lett.* **29,** 2127 (2002).
26. Paillard, D. Quaternary glaciations: From observations to theories. *Quat. Sci. Rev.* **107,** 11–24 (2015).
27. Rooney, A. D. *et al.* A Cryogenican chronology: Two long-lasting synchronous Neoproterozoic glaciations. *Geology* **43,** 459–462 (2015).
28. Abbot, D. S. & Pierrehumbert, R. T. Mudball: Surface dust and Snowball Earth deglaciation. *J. Geophys. Res.* **115,** D03104 (2010).
29. Abbot, D. S., Voigt, S. & Koll, D. The Jormungand global climate state and implications for Neoproterozoic glaciations. *J. Geophys. Res.* **116,** D18103 (2011).
30. Rose, B. E. J. Stable "Waterbelt" climates controlled by tropical ocean heat transport: A nonlinear coupled climate mechanism of relevance to Snowball Earth. *J. Geophys. Res.* **120,** 1404–1423 (2015).

Acknowledgements

This work was supported by the NERC-funded project GR3/ NE/H004963/1 Glacial Activity in Neoproterozoic Svalbard (GAINS). Logistical support was provided by the University Centre in Svalbard. This work was granted access to the HPC resources of CCRT under allocation 2014-017013 made by GENCI (Grand Equipement National de Calcul Intensif). We also thank D. Paillard and P. Hoffman for stimulating discussions and valuable insights.

Author contributions

Field data were collected and analysed by I.J.F., D.I.B., E.J.F., M.J.H., E.A.McM., M.S.P., P.M.W. and C.T.E.S. Geochemical analyses were conducted by H.B. and P.M.W. Model experiments were designed and conducted by G.L.H., Y.D., C.D. and G.R. The manuscript and figures were drafted by D.I.B., I.J.F. and G.L.H., with contributions from the other authors.

Additional information

Supplementary information is available in the online version of the paper. Reprints and permissions information is available online at www.nature.com/reprints. Correspondence and requests for materials should be addressed to D.I.B.

Competing financial interests

The authors declare no competing financial interests.

Methods

Sedimentology. Lithofacies were classified based on grain size, internal sedimentary structures and deformation structures, and bounding surfaces. Detailed stratigraphic logs were made in the field, supplemented by drawings and photographs of key features. Samples were taken for polishing and thin sectioning, to allow detailed examination of microstructures in the laboratory. In addition, data were collected on clast lithology, shape, surface features and fabric. Diamictites of the Wilsonbreen Formation are commonly very friable, allowing included clasts to be removed intact from the surrounding matrix, allowing measurement of both clast morphology and orientation, using methods developed for unlithified sediments. Clast morphology (shape, roundness and surface texture) was measured for samples of 50 clasts to determine transport pathways. Clast fabric analysis was performed by measuring a-axis orientations of samples of 50 clasts with a compass-clinometer, and data were summarized using the eigenvalue or orientation tensor method. Oriented samples for measurement of anisotropy of magnetic susceptibility (AMS) were collected using a combination of field-drilling and block sampling. AMS was measured using an AGICO KLY-3 Kappabridge operating at 875 Hz with a 300 A m^{-1} applied field at the University of Birmingham and an AGICO MFK-1A Kappabridge operating at 976 Hz with a 200 A m^{-1} applied field at New Mexico Highlands University.

Geochemistry. Laboratory procedures for extracting, purifying and measuring the triple oxygen ($\delta^{18}O$ and $\Delta^{17}O$) and sulphur ($\delta^{34}S$) isotope composition of carbonate associated sulphate (CAS) in bulk carbonates are detailed in ref. 16. Briefly, fresh carbonate-bearing rock chips were crushed into fine grains and powders using mortar and pestle. Rinsing the fines with 18 MΩ water revealed little water-leachable sulphate in any of the Wilsonbreen carbonates. Subsequently, about 10 to 30 g carbonates were slowly digested in 1–3 M HCl solutions. The solution was then centrifuged, filtered through a 0.2 μm filter, and acidified before saturated $BaCl_2$ droplets were added. $BaSO_4$ precipitates were collected after >12 h and purified using the DDARP method (see Supplementary Information). The purified $BaSO_4$ was then analysed for three different isotope parameters: $\Delta^{17}O$, by converting to O_2 using a CO_2-laser fluorination method; $\delta^{18}O$, by converting to CO through a Thermal Conversion Elemental Analyzer (TCEA) at 1,450 °C; and $\delta^{34}S$, by converting to SO_2 by combustion in tin capsules in the presence of V_2O_5 through an Elementar Pyrocube elemental analyser at 1,050 °C. The $\Delta^{17}O$ was run in dual-inlet mode, whereas the $\delta^{18}O$ and $\delta^{34}S$ were run in continuous-flow mode. Both the $\Delta^{17}O$ and $\delta^{18}O$ were run on a MAT 253 at Louisiana State University, whereas the $\delta^{34}S$ was determined on an Isoprime 100 continuous-flow mass spectrometer at the University of Lancaster, UK. The $\Delta^{17}O$ was calculated as $\Delta^{17}O \equiv \delta'^{17}O - 0.52 \times \delta'^{18}O$ in which $\delta' \equiv 1{,}000\ln(R_{sample}/R_{standard})$ and R is the molar ratio of $^{18}O/^{16}O$ or $^{17}O/^{16}O$. All δ values are in Vienna Standard Mean Ocean Water VSMOW and Vienna Canyon Diablo Troilite (VCDT) for sulphate oxygen and sulphur, respectively. The analytical standard deviation (1σ) for replicate analysis associated with the $\Delta^{17}O$, $\delta^{18}O$ and $\delta^{34}S$ are ±0.05‰, ±0.5‰ and ±0.2‰, respectively. As the CAS is heterogeneous in hand specimens, the standard deviation is for laboratory procedures. $\delta^{34}S$ values were corrected against VCDT using within-run analyses of international standard NBS-127 (assuming $\delta^{34}S$ values of +21.1‰). Within-run standard replication (1 s.d.) was <0.3‰. All geochemical data are included in Supplementary Table 1.

Numerical modelling. Model runs were conducted with a coupled atmospheric general circulation model (LMDz) and ice sheet model (GRISLI: GRenoble Ice Shelf and Land Ice model). LMDz (spatial resolution 4° in latitude × 5° in longitude with 38 vertical levels) was run with prescribed continental ice to climatic equilibrium. GRISLI has a 40 km grid size and is driven with downscaled climatic fields of surface air temperature, precipitation and evaporation. To capture ice sheet–climate feedbacks, LMDz is rerun using the new ice sheet distribution and topography. This procedure was repeated each 10 kyr to investigate orbital forcing.

Surface mass balance (accumulation minus sublimation and melting) was computed from monthly mean temperature, precipitation and evaporation rate. Melt rate is calculated using the positive-degree-day method.

No sea ice dynamics treatment is specified, the sea ice cover is prescribed and a thickness of 10 m is imposed. Ice albedo is fixed at 0.6, whereas snow albedo varies from 0.9 from 0.55 as a function of the zenith and ageing process. Land ice/snow free surface has the characteristic of a bare soil (rocky regolith) with an albedo of 0.3.

Code availability. Code for the GCM LMDz can be accessed at: http://lmdz.lmd.jussieu.fr. Code for the ISM GRISLI (GRenoble Ice Shelf and Land Ice model) is not available.

Further details of the methods and modelling procedures are provided in the Supplementary Information in the online version of the paper.